Ehrlich-Schwoebel effect for vacancies: Low-index faces of silver

Michael I. Haftel

Nanostructures Optics Section, Naval Research Laboratory, Washington, DC 20735-5343

We employ surface-embedded-atom-method potentials to investigate the energy landscape of vacancies diffusing over, along, and near steps on the low-index faces of silver. We compare the vacancy diffusion barriers with those of adatoms. Barriers for vacancies diffusing in the surface of terraces near and up close-packed step edges are calculated for the (111), (100), and (110) surfaces. Large Ehrlich-Schwoebel (ES) barriers (>200 meV) for vacancies ascending step edges occur on all three faces, and these barriers are enhanced over those of adatoms. Barriers for their diffusion along step edges and around kinks and corners of vacancy islands are calculated for the (100) surface. Here a sizable vacancy "corner" ES barrier occurs (148 meV). The "kink" ES barrier, which proceeds by the exchange mechanism, is very small (7 meV). We develop an accurate scheme of estimating the vacancy energy landscape in terms of bond breaking and atomic coordination at the relevant surface lattice sites. We assess the role of the vacancy diffusion barriers on the structure of two-dimensional (2D) vacancy islands and 3D vacancy pits on Ag(100). The vacancy ES effect promotes a pitted morphology that persists above room temperature. The calculated vacancy diffusion barriers do not support the suggestion that vacancy diffusion on top of clusters can help account for the behavior of the observed scaling exponent for the coarsening or diffusion of Ag clusters on Ag(100).

I. INTRODUCTION

The possibility of exploiting the controlled formation of tailor-made nanostructures on metal and semiconductor surfaces has spurred a renewed interest in two-dimensional (2D) and 3D island dynamics. While thermodynamic considerations such as strain play a paramount role in the self-assembly of 2D and 3D island structures, kinetic considerations such as diffusion barriers play important roles also, especially near step edges where key mass transport processes are taking place. For example, the Ehrlich-Schwoebel (ES) barrier[1]—i.e., the increase in energy for an adatom to diffuse over a step edge compared to the diffusion barrier on the flat terrace—is a key factor in 3D island dynamics mechanisms,[2,3] as well as having effects on 2D island dynamics and step phenomena.[4–6]

The influence of mass transport on island dynamics can involve the diffusion of vacancies as well as adatoms. In the formation phase, during the deposition or removal (e.g., by evaporation or sputtering) of atoms, we would expect the transport coefficients for adatoms and small clusters to play the dominant role in the former and those for vacancies to dominate the latter. In the subsequent consolidation or equilibration phase, either or both types of mass carriers can influence the morphological evolution of adatom *or* vacancy islands depending on their concentrations and mobilities. For example, vacancy diffusion has been shown to be the dominant mass transport mechanism on Cu(100) (Ref. 7) for the ripening of either adatom or vacancy islands. It has also been suggested, on the basis of kinetic Monte Carlo simulations for Cu(100), that vacancy diffusion across upper island terraces dominates the diffusion constant and scaling exponent for large Ag(100) *adatom* islands as well.[8] Given the complicated nature of the interatomic forces, the dominance of adatom or vacancy transport is hard to predict in advance and varies from surface to surface and between atomic spe-

cies. While many calculations exist for adatom diffusion barriers, this paper concentrates on calculating vacancy diffusion barriers on low-index Ag surfaces and especially on their behavior near island and step edges, including a possible vacancy ES barrier.

Many scanning tunneling microscopy (STM) studies have been carried out, especially on Ag surfaces, to investigate the formation, dynamics, and coarsening of adatom and vacancy islands and the underlying atomic transport processes. Several investigators[9–11] have observed the diffusion and coarsening of large Ag(100) islands, but the dominant transport mechanism—edge adatom diffusion[11] or a combination of edge diffusion and terrace vacancy diffusion[8]—is a subject of some controversy. Abnormally fast decay of islands in "wedding cake" configurations has been observed by Giesen *et al.*[12] for adatom islands and by Morgenstern *et al.*[13] for vacancy islands on Ag(111). These have suggested the effective disappearance of ES barriers when the edges of such double islands come close together. Hoogeman *et al.* observe, with STM, abnormally fast transfer of vacancies between vacancy islands when they are less than 20 Å apart, which they conjecture is the result of a strain enhancement of the vacancy diffusion constant.[14] All of these aforementioned processes involve the post-deposition (or removal) equilibration of the surface where both adatom and vacancy transport may contribute. To understand these processes and to assess the anomalies, knowledge of both adatom and vacancy transport constants are necessary, especially near step and island edges.

Pai and Reutt-Robey[15] report a dominant 3D vacancy island (pitting) morphology on Ag(100) with sufficient O_2 exposure. In sputtering experiments Constantini *et al.*[16] observe 3D pitting well above room temperature on Ag(110), well beyond the temperature at which 3D islands form for adatom islands in deposition. The former work suggests a vacancy ES barrier on Ag(110), while the latter investigators

TABLE I. SEAM vacancy and adatom surface formation energies, in meV, for the low-index faces of silver, and their equilibrium concentrations c_{eq} in nm^{-2} at 300 K. The number in parentheses indicates the power of 10.

| | Adatom | | Vacancy | |
	E_{SF}	c_{eq}	E_{SF}	c_{eq}
Ag (111)	847	4.07(−14)	758	1.27(−12)
Ag (100)	546	8.03(−9)	544	8.68(−9)
Ag (110)	283	1.49(−4)	226	1.35(−3)

have cited a vacancy ES effect as a possible explanation of their observations. Effective medium theory (EMT) calculations[17] predict a 0.24-eV-vacancy ES barrier on Ag(100), while embedded-atom-method (EAM) calculations[7] predict a 0.18-eV ES barrier on Cu(100). In our investigation of vacancy diffusion near step edges, one of the main purposes is to systematize these vacancy diffusion barriers for the Ag surfaces in a way that would apply to other metal surfaces as well. We will also indicate how knowledge of the vacancy diffusion near step edges impacts the understanding of some of the aforementioned observations.

This paper explores the "energy landscape" of vacancies on the low-index silver surfaces, i.e., the sequence of diffusion activation energies and site adsorption energies a vacancy encounters as it diffuses along the terrace or over or along step edges. We employ the surface-embedded-atom method[18] (SEAM) for Ag to calculate these energies. Section II describes the calculation of the vacancy energy landscape using this potential. Section III gives the energy landscapes for vacancies diffusing near and along step edges and morphological consequences. We illustrate the role of the adatom and vacancy ES barrier in producing pitted morphologies on low-index Ag faces. A simple model is proposed involving bond breaking and initial- and final-state coordination to account for the calculated energy landscapes. We show how the vacancy ES effect can help account for the observation of 3D vacancy island growth on Ag surfaces. Using our calculated energy landscapes, we discuss their implications on 2D vacancy island shapes and the outstanding issues concerning the diffusion and coarsening of large clusters on Ag(100).

II. SEAM MODEL OF VACANCY DIFFUSION BARRIERS

We employ the SEAM potential AG1 of Ref. 18 in our calculations of surface energetics. The formal description of the potential is the same as in the embedded-atom method, except that the pair potential is of a general form, more in keeping with the glue model of Ercolessi et al.[19] The parameters of the potential are fit to surface energies and low-index reconstructions in addition to the usual bulk properties (cohesive energy, lattice and force constants, etc.). The terrace diffusion and ES barriers predicted by this potential[20] are in good agreement with those measured experimentally on Ag(111) (Refs. 3 and 21) and Ag(100) (Refs. 22–24).

Before we address the question of the energy landscape, we will address the question of whether vacancy transport can be important factor in island dynamics. Table I gives the

SEAM surface adatom and vacancy formation energies, and corresponding room-temperature equilibrium concentrations, for the three low-index faces of Ag. On all three faces the vacancy equilibrium concentration is higher than that for adatoms [albeit only slightly higher on (100)]. Therefore equilibrium concentrations of vacancies will be as high as or higher than those of adatoms. While these concentrations are low on the atomic scale, they are sufficient to drive the diffusion and coarsening of large ($N > 100$) islands, which are typically observed by STM over periods of hours.[9–11]

We compute both adatom and vacancy diffusion activation energies as described in previous work.[20] The main difference is that a vacancy diffuses in the surface layer, while an adatom diffuses above the surface. Physically, the diffusion of a vacancy from sites A to B corresponds to a surface atom diffusing from site B to the site of the former vacancy at A. Thus the basic hyperplane search used in Ref. 20, utilizing the conjugate gradient method, can be employed unmodified except we now move surface atoms rather than adatoms, employing the SEAM potential to calculate total energies. For exchange diffusion we must consider alternate pathways between initial and final state to find the one with the minimum saddle-point energy. As in the previous investigation,[20] we estimate the numerical uncertainty of our barriers as ~2 meV for hopping processes and ~10 meV for exchange processes. This represents just the error coming from the hyperplane search. An additional uncertainty exists from using a semiempirical potential.

Different EAM potentials[25] can predict different values for the same diffusion constant differing by a factor of 2, but generally reproduce the relative trends of different diffusion constants that are obtained from experiment or first-principles calculations. Our SEAM potentials give much better description of surfaces than most other EAM potentials, and for adatoms on low-index Ag surfaces the diffusion barriers typically differ by 10%–15% from experimental values, where available.[20] From the EAM model of Adams et al.,[25] Mehl et al.[26] calculate and systematize, for several metal fcc (100) surfaces including Ag, a set of diffusion barriers including some of the vacancy diffusion processes we consider. The present work differs in that we consider the full vacancy energy landscapes near step edges, corners, and kinks. Furthermore, some of the barriers we calculate with the SEAM differ appreciably from those predicted by EAM (Ref. 26) and EMT (Ref. 17) calculations. The Ag(111) SEAM adatom diffusion energy of 0.12 eV and ES barrier of 0.14 eV are in good agreement with experimental determinations of 0.10 eV (Ref. 21) and 0.12 eV (Ref. 3), respectively. The SEAM predicts a 0.038-eV ES barrier on Ag(100) going by exchange diffusion (see next section, Table II), whereas EMT (Ref. 17) indicates a 0.11-eV barrier going by hopping. The near vanishing of this barrier by exchange is favored by the experiment of Suziki et al.[27] and density-functional calculations.[28] However, experiments and simulations by Zhang et al.[23] and Stoldt and co-workers[29,30] indicate that an ES barrier of 0.03–0.06 eV can help account for the observed roughness of the Ag(100) surface at ~200 K. To our
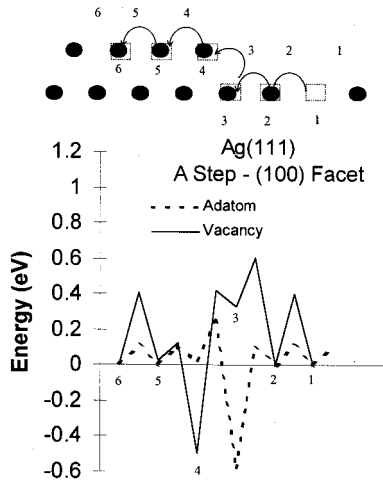
FIG. 1. Vacancy energy landscape (solid line) as it diffuses from the lower terrace (from site 1) over the Ag(111) *A*-step edge (to site 6). The straight lines just connect vacancy sites with neighboring saddle points. The dotted line gives the adatom landscape for comparison, connecting fcc sites with neighboring saddle points. The diagram gives a schematic side view of the vacancy diffusing over the step edge. The lower set of numbers on the graph corresponds to the set of numbers at the vacancy sites on the diagram. The upper numbers on the diagram indicate the fcc adsorption sites.

knowledge direct measurements or first-principles calculations of the Ag vacancy diffusion barriers do not presently exist.

III. RESULTS

Usually, surface vacancy diffusion on the terrace requires the breaking of more bonds (by the moved atom) than adatom diffusion above the surface. This suggests that vacancies should be less mobile than adatoms. However, the bonds are broken in an environment with a higher coordination where the bonds are weaker. Thus it is hard to judge the mobility without an actual calculation. On the basis of our calculations, we will later propose some simple bond-counting rules to estimate vacancy diffusion landscapes.

Figure 1 illustrates the SEAM energy landscape for a vacancy diffusing on the Ag(111) surface starting from traversing the lower terrace and proceeding up the *A*-step edge (100 microfacet). The landscape for diffusing adatoms is included for comparison. Figure 2 gives the landscapes for the *B*-step edge (111 microfacet). Table II compares the terrace and step-edge diffusion energies of adatoms and vacancies, and the excess (ES) barriers over steps, corners, and kinks, for the considered low-index faces of Ag. Vacancies are much less mobile than adatoms with a terrace vacancy diffusion energy of 404 meV (versus 117 meV for adatoms) on Ag(111), and the vacancy landscapes are rather similar for the *A* and *B* steps. When the vacancy moves from site 2 to site 3, attaching to the bottom of the step, the moved atom moves from site 3 to site 2, requiring the breaking of a bond with the atom in site 4 in addition to the usual breaking of surface bonds. Thus a higher [606 meV (*A*), 630 meV (*B*)] barrier is obtained. Site 3 is a site of tenfold atomic coordi-
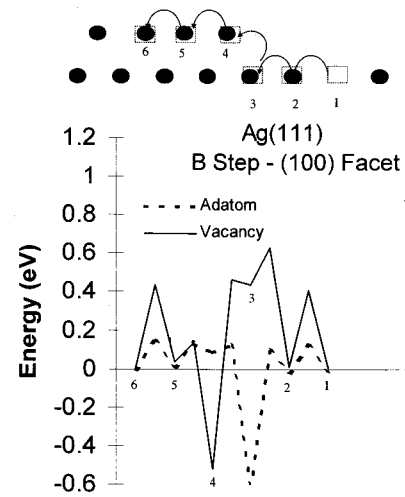
FIG. 2. Vacancy (solid line) and adatom (dotted line) energy landscape near the Ag(111) *B*-step edge. The diagrams and symbols have the same meaning as in Fig. 1.

nation, as opposed to ninefold in the terrace, and is metastable as vacancies, in contradistinction to adatoms, prefer sites of low coordination. The vacancy is strongly "bound" to the top of the step edge, site 4, as this site has lower (sevenfold) atomic coordination. The vacancy easily climbs the step edge (to site 4) with a barrier of 92 meV (*A*) or 28 meV (*B*). Thus the maximum energy barrier encountered is 606 meV (*A*) [630 meV (*B*)] when the vacancy diffuses over the lower terrace and up the step edge. The difference between this energy and the vacancy terrace diffusion energy (away from the step)—202 meV (*A*) [226 meV (*B*)]—is the vacancy Ehrlich-Schwoebel barrier ΔE_{ES} and is so indicated in Table II. Unlike its adatom analog, the ES barrier is encountered immediately before the interlayer transport rather than during. The ES barrier will produce a downhill vacancy current or, correspondingly, an uphill mass current and promote pitting and mounding.

If we look at Fig. 1 for a vacancy diffusing on the top terrace, eventually attaching to the top of the step edge at site 4, there is a large decrease in the diffusion barrier on attachment, i.e., when the vacancy diffuses from site 5 to site 4. When the corresponding atom moves from sites 4 to 5, fewer bonds are broken (two) than in terrace vacancy diffusion (three), and this vacancy "attachment" barrier is significantly lower than the terrace diffusion energy. The increase or decrease in the attachment barrier over the terrace diffusion energy is denoted as ΔE_{att} in Table II. A large negative ΔE_{att} [−280 meV (*A*), −264 meV (*B*)] is a rather striking feature of the energy landscape for vacancies, much more so than its adatom counterpart.

The energy landscapes of Figs. 1 and 2 can be semiquantitatively accounted for from simple bond-counting arguments. We illustrate with the *A*-step results. The energies at the vacancy adsorption sites increase approximately linearly in the atomic coordination of site, with a proportionality constant 250–320 meV. For example, the terrace sites have ninefold atomic coordination, whereas site 4 has sevenfold coordination and an energy decrease of 494 meV. As for vacancy diffusion in the open terrace, three of the five surface bonds

TABLE II. SEAM adatom and vacancy terrace diffusion energies (E_{TD}), step-edge Ehrlich-Schwoebel barriers (ΔE_{ES}), step-attachment barriers (ΔE_{att}), edge diffusion energies (E_{edge}), and corner and kink Ehrlich-Schwoebel barriers ($\Delta E_{CES}, \Delta E_{KES}$). All energies are defined in the text and figures, and are expressed in meV. When two numbers appear for Ag (111), the first refers to the A step, the second to the B step. The Ag (110) results are for diffusion between close-packed rows. Underlined numbers indicate that the process goes by exchange diffusion.

	Ag (111)		Ag (100)		Ag (110)	
	Adatom	Vacancy	Adatom	Vacancy	Adatom	Vacancy
$E2TD$	119	404	$\underline{402}$	473	$\underline{323}$	$\underline{668}$
ΔE_{ES}	139 6	202 226	39	248	$\underline{383}$	$\underline{367}$
ΔE_{att}	-54 -25	-280 -264	-26	-230	$\underline{19}$	$\underline{10}$
E_{edge}			294	472		
ΔE_{CES}			$\underline{213}$	148		
ΔE_{KES}			$\underline{118}$	$\underline{7}$		

are broken for the moved atom going to the transition state, e.g., in the vacancy diffusion from site 1 to 2 (with an atom moving from 2 to 1), with a diffusion barrier of ~400 meV. Hence a cost of approximately 130 meV can be associated with the breaking of a surface bond. Also, when there is a change between initial- and final-state atomic coordination, the forming of additional (fewer) bonds significantly decreases (increases) the diffusion energy. For example, for vacancy diffusion between sites 4 and 5, three surface bonds are broken as in vacancy terrace diffusion, but the diffusion atom 5 has initial-state coordination 8 and final-state coordination 6, a decrease of 2. The diffusion barrier here is 618 meV, 218 meV higher than the vacancy diffusion barrier. Therefore the gain or loss of atomic coordination costs approximately the same as breaking surface bonds.

The above explanation of the energy landscape can be approximately described by the relations

$$E_i = 2E_0(C_i - C_T), \tag{1a}$$

$$\Delta E_{ij} = E_0(S_{Bji} + C_j - C_i), \tag{1b}$$

where E_i is the energy with a vacancy at site i relative to that on the terrace away from the step, C_i the atomic coordination of the site, and C_T the atomic coordination of a site on the open terrace. In Eq. (1b), ΔE_{ij} is the diffusion activation barrier for a vacancy diffusing from site i to j, and S_{Bji} the number of "surface" bonds broken when an atom is moved from site j to i. Surface bonds include all nearest-neighbor bonds at least partially exposed to the surface. They would include the partially vertical bond between atoms at sites 3 and 4 and the partially exposed surface bond between an atom at site 3 and the nearest-neighbor atom on the same level just below the step edge. The breaking of bonds with the subsurface is not taken into account, although they may have some minor influence. For Ag(111), $C_T = 9$ and we take $E_0 = 130$ meV. Table III gives the comparison between the estimates of Eq. (1) and the SEAM-calculated energy landscape. The agreement is quite good, even when interlayer transport is involved. Normally, bond-counting arguments do not account for the ES barrier in adatom diffusion because (as in Ag) the process goes by exchange. Equation (1) does not apply to exchange diffusion, which is generally less fa-

TABLE III. Energy landscape for a vacancy diffusing in the surface of Ag (111) from sites 1 to 6 of Fig. 1, as predicted by Eq. (1) and as calculated by the SEAM. The E_0 parameter for Ag (111) is 130 meV. Here E_{ij} is the saddle-point energy between sites i and j, i.e., $E_{ij} = E_i + \Delta E_{ij}$ of Eq. (1). All energies are in meV.

i					E (SEAM)	
i j	C_i	S_{Bji}	E [Eq. (1)]		A step	B step
1	9		0		0	0
1 2		3	390		398	411
2	9		0		1	1
2 3		4	650		606	624
3	10		260		326	430
3 4		4	390		418	458
4	7		-520		-494	-527
4 5		3	130		124	134
5	9		0		26	30
5 6		3	390		404	433
6	9		0		-1	-6
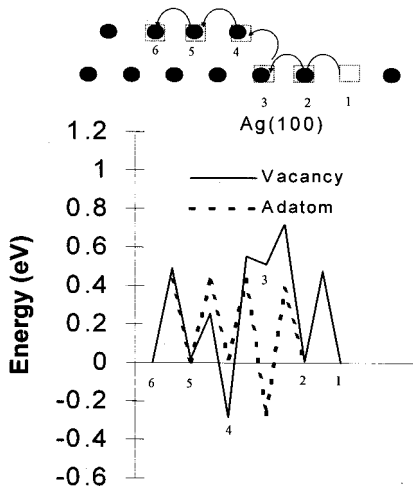
FIG. 3. Vacancy and adatom landscapes near the Ag(100) step edge. Symbols and layout are the same as in Fig. 2.

FIG. 4. Critical and average adatom and vacancy island radii for nucleation of 3D islands or pits on Ag(100) using the theory of Ref. 32. Results are for coverage of 0.25 ML, deposition or evaporation flux of 0.01 ML/s, and a critical island size of $i_c = 1$.

vorable for vacancy diffusion processes than it is for adatom diffusion.

Do the trends observed for vacancy diffusion on Ag(111) carry over to the other low-index faces? Figure 3 illustrates the corresponding energy landscape for Ag(100). The features are qualitatively similar to Ag(111) with a metastable state when the vacancy is attached to the bottom of the step edge and a strongly bound state when attached at the top. Unlike on Ag(111), vacancies are only slightly less mobile on Ag(100) than adatoms (473 meV versus 405 meV) on the terrace. The SEAM result suggests that vacancies are not as mobile on Ag(100) as predicted in the EAM (360 meV) (Ref. 26) or EMT (412 meV) (Ref. 17) calculations. The vacancy ES barrier of 248 meV occurs again on the attachment to the lower step edge just before the interlayer transport of the vacancy up the step edge. The diffusion energy of a vacancy on Ag(100) is similar to that of an adatom (see Table II), but the ES barrier ΔE_{ES} is much larger than for an adatom (Table II). Likewise, ΔE_{att} for a vacancy is very large (unlike that for adatoms) and negative, which facilitates attachment to the top of the step edge from the top terrace.

One difference between vacancy and adatom diffusion on Ag(100) is that, similar to Ag(111), exchange diffusion does not play a role in vacancy diffusion on the terrace or over the step edge (see Table II). Our equations (1), with $E_0 = 140$ meV, does a good job in estimating the energy landscape. The largest error comes in estimating the ES barrier, which is overestimated (560 meV versus 248 meV).

The large ES barrier on Ag(100) promotes a large downhill (uphill) vacancy (mass) current. In analogy to the adatom ES effect promoting 3D growth, the vacancy ES effect should promote 3D vacancy island growth, i.e., pitting, as suggested in Ref. 16. Figure 4 illustrates the role of the vacancy ES barrier in 3D vacancy island growth (pitting) on Ag(100) and a corresponding plot for adatoms. This figure plots the average 2D island radius and the critical radius for 3D island formation for vacancy and adatom islands as functions of temperature. The average radius, which depends on the incident flux, coverage, and temperature, is obtained
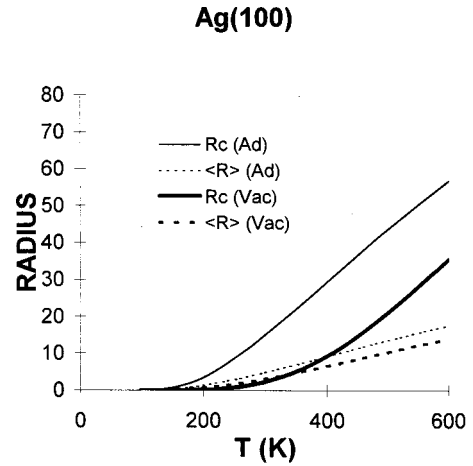
from nucleation theory.[31] We define the critical radius similar to Ref. 3, i.e., the island radius on top of which stable clusters start to nucleate. Our estimate of the critical radius for 3D island formation utilizes the nucleation frequency ω given by Eq. (13) of Krug et al.[32] to determine a critical radius of a 2D island at which one island of critical size $i_c + 1$ will be nucleated on top of it, i.e., $\omega t = 1$, and t is the deposition time. For purposes of illustration we take an incident or evaporation flux of 0.01 monolayer per second (ML/s), a coverage of 0.25 ML, and all diffusion prefactors of 1.0 THz. We also assume stable divacancies and dimers (i.e., $i_c = 1$). The vacancy ES effect here accounts for a very small critical radius to well above room temperature. Under the assumed conditions the transition temperature for 3D to 2D growth (i.e., where R_c becomes more than $\langle R \rangle$) does not occur until 340 K for vacancies as compared to 120 K for adatoms. In sputtering experiments Constantini et al.[16,33] observe considerable 3D pitting up to about 350 K compared to 3D island formation cutting off at about 220 K in comparable deposition experiments. The above results confirm that the vacancy ES effect considerably facilitates pitting on Ag(100) above room temperature as well.

The results in Fig. 4 illustrate the important role of the vacancy ES effect in 3D pitting. The ES barriers we used are taken directly from the SEAM for interlayer transport over a close-packed $\langle 110 \rangle$ straight step edge. We did not consider possibly enhanced interlayer transport over thermally roughened step edges.[30,34] We also calculated the critical radius using the earlier treatment of Tersoff et al.[2] The results are qualitatively similar to those of Fig. 4, but differ quantitatively in that the transition temperatures become 140 and 420 K for adatom and vacancy islands, respectively. Krug et al.[32] and Heinrichs et al.[35] argue that the rate equation approach[2] has a limited range of validity, especially when the nucleation on top of islands is a rare event.

Ag(110) has a quite different energy landscape than the (100) and (111) faces, owing to its lower symmetry. Figure 5 depicts the energy landscape for a vacancy on Ag(110) near
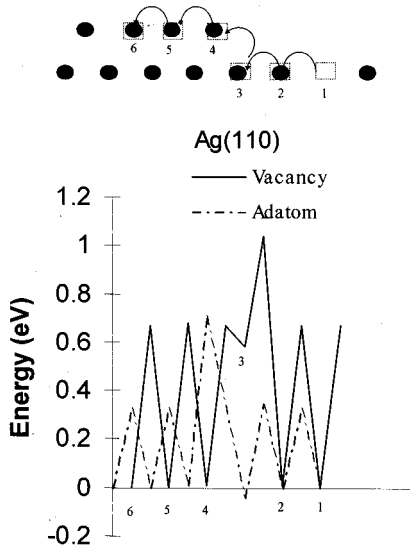
FIG. 5. Vacancy and adatom energy landscapes near the Ag(110) step edge. The close-packed rows go into the paper.

FIG. 6. Vacancy energy landscape as it diffuses along and around the corner of a step edge of a vacancy island on Ag(100). The diagram is a top view with dark circles representing upper-terrace atoms and the white circles representing the top layer of the vacancy island. The dashed line on the diagram and graph indicates the exchange path 2-4.

and over a close-packed step. Migration *between* close-packed rows goes by exchange because of the open nature of the (110) surface, with a barrier of 668 meV. Migration *along* the close-packed rows goes by hopping with a barrier of 454 meV. The ES barrier is the highest studied with $\Delta E_S = 367$ meV. A striking feature of Fig. 5, besides the very large ES barriers, is that vacancies do not bind to step edges, nor is there a significant ΔE_{att}. These features are present in the adatom landscape as well and result from the bonds between close-packed rows being weak second-nearest-neighbor bonds. The step edge, on both the upper and lower terraces, acts as a reflecting barrier for both and vacancies and adatoms on Ag(110).

The large ES barrier for vacancies on Ag(110) facilitates pit formation under evaporation conditions. Large pits have been observed with STM on Ag(110) with large O_2 exposure.[15] Here the vacancy ES effect causes a downhill vacancy current maintained by single atom vacancies produced by the impinging O_2 molecules, with the resultant pitting. An interesting feature of these observations[15] is a "depletion zone" of ~1600 Å from the step edge on the lower terrace. As pointed out by Kandel,[4] in the absence of an adatom attachment barrier on the lower terrace, the step edge acts like a perfect sink for lower terrace adatoms, especially if the binding to the step edge is large, which will lead to a decreased adatom concentration, or depletion zone, on the lower terrace near the step edge. By the same token we would normally expect a depletion zone of vacancies near the *upper* step edge. Unlike the other low-index faces, however, vacancies do not bind there on Ag(110); thus, no depletion zone would be expected there, nor is one observed.[15] For vacancies we would normally expect enhanced pitting on the lower terrace near the step edge due to the increased collisional flux of vacancies reflecting off the step edge from the ES effect, but just the opposite is observed.[15] Here the effect of the increased collisional flux is suppressed because the vacancies are quite immobile compared to adatoms (Fig. 5,
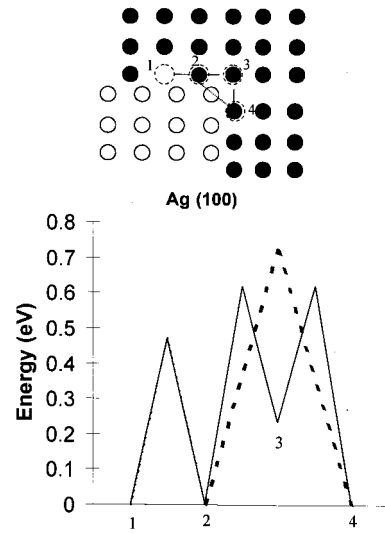
Table II), and these mobile adatoms are emitted from the step edges (most likely from kink sites) at a rate fast enough to annihilate the nearby vacancies before they can nucleate.

We now consider vacancy diffusion along the step edge of vacancy islands and examine the features of the analogous ES effects at corner and kinks. Step-edge diffusion is known to influence island shapes as easy edge diffusion in relation to terrace diffusion promotes compact island shapes, while the opposite promotes fractal shapes.[36,37] This holds for vacancy islands as well. Edge diffusion can also be the primary transport mechanism in the diffusion of large adatom or vacancy clusters.[11] Furthermore, recent investigations have shown that the 2D analogs to the ES barrier, i.e., the extra energy needed to diffuse around a corner or kink of a step edge, have profound influences on 3D growth and step fluctuations as well.[38,39] We now assess the role that vacancy diffusion plays in these processes.

Figure 6 illustrates the landscape encountered by vacancies migrating along the Ag(100) step edge and rounding corners of vacancy islands. These are compared to the corresponding adatom quantities in Table II, in which ΔE_{CES} is the extra energy needed to diffuse around the corner. All the diffusion energies shown are well described by Eqs. (1) with $E_0 = 140$ meV.

The vacancy edge diffusion energy is slightly higher than on the terrace (472 meV versus 404 meV), but much higher than that of adatoms (294 meV), and a metastable site occurs at the corner where the atomic coordination increases. A corner vacancy ES (CES) barrier occurs because the atom originally in site 3 loses a nearest-neighbor bond when it moves to site 2, whereas the number of exposed surface bonds broken is 3 for either vacancy diffusion path 1-2 or 2-3. Our SEAM vacancy edge diffusion and additional corner barriers are close to the EAM values.[26] Figure 6 also illustrates va-
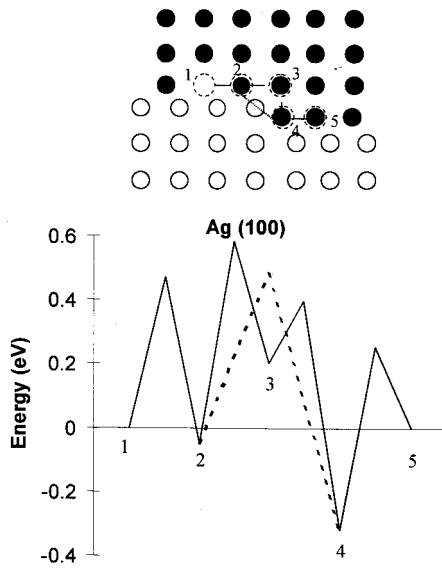
FIG. 7. Vacancy energy landscape as it diffuses along and around a kink of a step edge of a vacancy island on Ag(100). The dashed line on the diagram and the graph indicates the exchange path 2-4.

cancy corner rounding by the ''shortcut'' 2-4 with the exchange mechanism. This path is 99 meV more expensive than the path 2-3-4 around the corner. The shortcut exchange path, however, is preferable for adatoms rounding corners (Table II).

As previously noted, island shapes are primarily influenced by the facility of periphery diffusion versus terrace diffusion (TD).[36,37] Easy diffusion around the island periphery favors compact shapes: difficult periphery diffusion favors fractal shapes. As pointed out by Zhang *et al.*,[37] periphery diffusion is influenced by the diffusion around corners as well as diffusion along the straight step edge. The CES effect additionally favors fractal shapes, and a large CES barrier renders the corner-rounding barrier ($E_C = E_{edge} + \Delta E_{CES}$) as the rate-determining process in mass transport around island edges. We expect that the higher edge diffusion barriers (relative to those of TD) for vacancies would yield less compact vacancy island shapes at a given temperature than those of adatoms. However, the smaller ΔE_{CES} for vacancies would mollify this effect. Then E_C is still less for adatoms than vacancies (507 meV versus 620 meV, Table II), but the determining factor $E_C - E_{TD}$ is only slightly less for adatoms (103 meV) than for vacancies (147 meV). We have applied the formulation of Zhang *et al.*[37] with our diffusion barriers to study the fractal-compact shape transition. The results indicate that both adatom and vacancy islands on Ag(100) should be compact at room temperature, but below 200 K the vacancy islands would tend more toward fractal shapes than adatom islands.

The energy landscape for vacancy edge diffusion in the presence of a kink is illustrated in Fig. 7. A kink ES (KES) barrier of 111 meV arises for the 2-3-4 pathway in the same way as the CES barrier previously discussed. This is close to the additional barrier of 130 meV calculated in Ref. 24, where no distinction is made between diffusion around a

corner and a kink. However, now the shortcut path 2-4 is preferable as the exchange barrier is now 104 meV cheaper than the hopping 2-3-4 path, lowering ΔE_{KES} to only 7 meV. The exchange process is more favorable than it is for the shortcut corner diffusion of Fig. 6 because the moved atom in site 4 has one fewer surface bond to break: i.e., there is no surface atom in the position of site 5 of Fig. 6. Furthermore, exchange diffusion may benefit from the occupied upper terrace sites that are nearest neighbors of the final site. Haftel and Rosen[20] find a dramatic lowering of the exchange barriers for Au/Ag(111) when an adatom occupies a nearest-neighbor site to the final site of the atom ejected from the surface: i.e., this nearby adatom catalyzes the exchange diffusion. The present result indicates that step edges also catalyze exchange diffusion events by lowering the exchange barrier.

The elimination of the vacancy KES barrier also eliminates the directionality of the mass flow coming from vacancies, i.e., the ''up-kink'' mass flow (that is, in the direction from site 2 to site 5 in Fig. 7) that the KES effect would normally produce.[30] By itself this would repress short-wavelength step fluctuations. The adatom KES effect would still contribute to the kinetic asymmetry, owing to the larger mobility of adatoms along the step edge. However, allowing the vacancy kinetics to dominate, for example by an evaporation flux, could help ''straighten'' steps.

As a final illustration of the role of the vacancy diffusion energy landscapes calculated here, we comment on the diffusion and coarsening scaling exponents for large clusters on Ag(100). In the post-deposition phase, the islands diffuse and coarsen. The diffusion constant scales according to $D \sim R^{-\alpha}$, where R is the island size and α is the scaling exponent. The islands coarsen according to $\langle N \rangle \sim t^{2\beta}$, where $\beta = 1/(\alpha + 2)$. Pai *et al.*,[10] in STM observations of diffusion and coarsening, determine that $\alpha \approx 2.3$ for clusters of 100–500 atoms. On the other hand, Stoldt *et al.*,[11] in STM observations of island coalescence, get $\alpha \approx 2.5 - 3.0$ as clusters decrease in size from 270 to 40 atoms (see their Fig. 4). On the basis of kinetic Monte Carlo simulations, it has been suggested[8] that a combination of *adatom* edge diffusion and *vacancy* terrace diffusion (on top of the adatom island) account for this intermediate behavior. Others argue against this view. A dominance of periphery diffusion mechanisms in island diffusion and coalescence on Ag(100) is advanced in Ref. 11 as well as in investigations of island coalescence on Ag(111) (Ref. 40) and in the decay of islands attached to step edges on Ag(100) (Ref. 41).

What do the SEAM energy landscapes suggest about the scaling? Khare and Einstein[5] give the cluster diffusion constants and scaling exponents in terms of the underlying diffusion constants in their equations (12) and (19). Using these expressions and the SEAM diffusion barriers and equilibrium densities—and using an attempt frequency of 1.0 THz as well as the kinetic coefficients as derived by Kandel[4]—we obtain the cluster diffusion constants on Ag(100) depicted in Fig. 8. We separate the adatom and vacancy diffusion contributions to the *adatom* cluster diffusion constants and also indicate the results if edge diffusion alone is considered. The effective scaling exponents $\alpha(N)$ indicated at $N = 100, 500,$
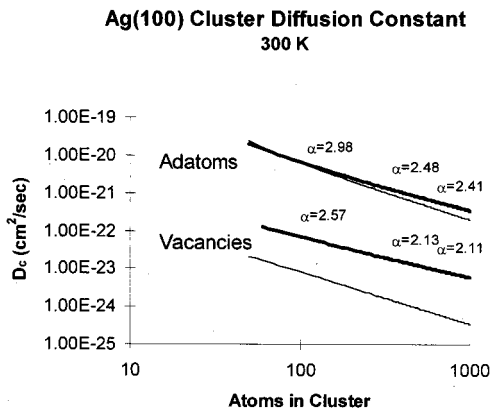
FIG. 8. Adatom and vacancy contributions to the cluster diffusion constants at 300 K on Ag(100), using SEAM diffusion barriers and Eq. (12) of Ref. 5. The dark lines utilize all the diffusion constants, whereas the lighter lines utilize the edge diffusion only.

and 1000 are defined from the relation $\alpha(N) = d\ln D_C/d\ln N$. For the range $N=100-300$, the scaling exponent is in good agreement with the observations of Stoldt et al.[11] It is clear from this figure that the diffusion of vacancies contributes negligibly to the total cluster diffusion constant and that edge diffusion of adatoms dominates, but that adatom terrace diffusion does help decrease the exponent at large N. Vacancies are too immobile, with the terrace diffusion and edge diffusion barriers 0.18 eV higher than the edge diffusion barrier for adatoms, to affect the coarsening kinetics of Ag clusters on Ag(100). The fact that the edge diffusion barrier for adatoms is 0.11 eV lower than the terrace diffusion barrier accounts for its dominance over most of the plotted range in Fig. 8.

IV. CONCLUSIONS

In conclusion, we have examined, for the low-index faces of Ag, the vacancy diffusion landscape near and around step and island edges that influence island and step growth and morphology. A primary finding is that a large vacancy ES barrier appears on all low-index faces of Ag, including (100)

where the ES barrier is very low for adatoms. The ES barriers, as well as the rest of the vacancy energy landscape near step edges, are well accounted for by the bond-breaking and coordination arguments summarized in our equations (1) and should appear also for other fcc metals. Furthermore, the barriers for vacancy attachment to the top of step edges are much lower than their terrace diffusion barriers. The observations of pitted morphologies on Ag(100) and Ag(110) are consistent with the vacancy ES effect. Vacancies are also significantly less mobile than adatoms on the open (100) terrace (barrier=473 meV) and along step edges (barrier =472 meV). This means that adatom diffusion (mainly around island edges) will dominate mass transport in both adatom and vacancy island decay, coarsening, and diffusion on Ag(100).

The 1D analog to the ES barrier around vacancy island corners exists ($\Delta E_{CES}=148$ meV) on Ag(100), but is much repressed around kinks on step edges ($\Delta E_{KES}=7$ meV), whereas both types of barriers exist for adatoms. The KES barrier all but disappears as the exchange mechanism becomes favorable to hopping for this process, perhaps because the nearby step edge "catalyzes" the exchange process. Analytic calculations here have indicated that the vacancy ES barrier can greatly influence adatom and vacancy island morphology, specifically promoting pitted morphologies at room temperature under mass-removal (e.g., evaporation, sputtering) conditions. Monte Carlo calculations utilizing these diffusion barriers could clearly verify their role.

[1] G. Ehrlich and F. G. Hudda, J. Chem. Phys. **44**, 1039 (1966); R. L. Schwoebel and E. J. Shipsey, J. Appl. Phys. **37**, 3682 (1966); R. L. Schwoebel, ibid. **40**, 614 (1969).

[2] J. Tersoff, A. W. Denier van der Gon, and R. M. Tromp, Phys. Rev. Lett. **72**, 3843 (1994).

[3] Karsten Bromann, Harald Brune, Holger Röder, and Klaus Kern, Phys. Rev. Lett. **75**, 677 (1995).

[4] D. Kandel, Phys. Rev. Lett. **78**, 499 (1997).

[5] S. V. Khare and T. L. Einstein, Phys. Rev. B **54**, 11 752 (1996).

[6] G. S. Bales and A. Zangwill, Phys. Rev. B **41**, 5500 (1990); Hyeong-Chai Jeong and Ellen D. Williams, Surf. Sci. Rep. **35**, 171 (1999).

[7] J. B. Hannon, C. Klünker, M. Giessen, H. Ibach, N. C. Bartelt, and J. C. Hamilton, Phys. Rev. Lett. **79**, 2506 (1997).

[8] J. Heinonen, I. Koponen, J. Merikoski, and T. Ala-Nissila, Phys. Rev. Lett. **82**, 2733 (1999).

[9] J. M. Wen, S.-L. Chang, J. W. Burnett, J. W. Evans, and P. A. Thiel, Phys. Rev. Lett. **73**, 2591 (1994); J. M. Wen, J. W. Evans, M. C. Bartelt, J. W. Burnett, and P. A. Thiel, ibid. **76**, 652 (1996).

[10] W. W. Pai, A. K. Swan, Z. Zhang, and J. F. Wendelken, Phys. Rev. Lett. **79**, 3210 (1997).

[11] C. R. Stoldt, C. J. Jenks, P. A. Thiel, A. M. Cadilhe, and J. W. Evans, J. Chem. Phys. **111**, 5157 (1999).

[12] M. Giesen, G. Schulze Icking-Konert, and H. Ibach, Phys. Rev. Lett. **80**, 552 (1998); M. Giesen and H. Ibach, ibid. **85**, 469 (2000).

[13] K. Morgenstern, G. Rosenfeld, G. Cosma, E. Lægsgaard, and F.

Besenbacher, Phys. Rev. Lett. **85**, 468 (2000).

[14] M. S. Hoogeman, M. A. J. Klik, R. van Gastel, and J. W. M. Frenken, J. Phys.: Condens. Matter **11**, 4349 (1999).

[15] W. W. Pai and J. E. Reutt-Robey, Phys. Rev. B **53**, 15 997 (1996).

[16] G. Constantini, R. Rusponi, R. Gianotti, C. Boragno, and U. Valbusa, Surf. Sci. **416**, 245 (1998).

[17] J. Merikoski, I. Vittolainen, J. Heinonen, and T. Ala-Nissila, Surf. Sci. **387**, 167 (1997).

[18] M. I. Haftel, Phys. Rev. B **48**, 2611 (1993); M. I. Haftel and M. Rosen, *ibid.* **51**, 4426 (1995).

[19] F. Ercolessi, E. Tosatti, and M. Parrinello, Phys. Rev. Lett. **57**, 719 (1986).

[20] M. I. Haftel and M. Rosen, Surf. Sci. **407**, 16 (1998).

[21] H. Brune, H. Röder, C. Boragno, and K. Kern, Phys. Rev. Lett. **73**, 1955 (1994).

[22] M. H. Langelaar, M. Breeman, and D. O. Boerma, Surf. Sci. **352−354**, 597 (1996).

[23] C.-M. Zhang, M. C. Bartelt, J.-M. Wen, C. J. Jenks, J. W. Evans, and P. A. Thiel, Surf. Sci. **406**, 178 (1998).

[24] L. Bardotti, C. R. Stoldt, C. J. Jenks, M. C. Bartelt, J. W. Evans, and P. A. Thiel, Phys. Rev. B **57**, 12 544 (1998).

[25] M. S. Daw and M. I. Baskes, Phys. Rev. B **29**, 6443 (1984); J. B. Adams, S. M. Foiles, and W. G. Wolfer, J. Mater. Res. **4**, 102 (1989).

[26] H. Mehl, O. Biham, and I. Furman, Phys. Rev. B **60**, 2106 (1999).

[27] Y. Suzuki, H. Kikuchi, and N. Koshizuka, Jpn. J. Appl. Phys., Part 2 **27**, L1175 (1988); W. C. Elliott, P. F. Miceli, T. Tse, and P. W. Stephens, Physica B **221**, 65 (1996); Phys. Rev. B **54**, 17 938 (1996).

[28] B. D. Yu and M. Scheffler, Phys. Rev. Lett. **77**, 1095 (1996).

[29] C. R. Stoldt, K. J. Caspersen, M. C. Bartelt, C. J. Jenks, J. W. Evans, and P. A. Thiel, Phys. Rev. Lett. **85**, 800 (2000).

[30] K. J. Caspersen, C. R. Stoldt, A. R. Layson, M. C. Bartelt, P. A. Thiel, and J. W. Evans, Phys. Rev. B **63**, 085401 (2001).

[31] J. G. Amar, F. Family, and P.-M. Lam, Phys. Rev. B **50**, 8781 (1994).

[32] J. Krug, P. Politi, and T. Michely, Phys. Rev. B **61**, 14 037 (2000).

[33] G. Constantini, F. Buatier de Mongeot, C. Boragno, and U. Valbusa, Phys. Rev. Lett. **86**, 838 (2001).

[34] U. Kuprick and T. S. Rahman, Phys. Rev. B **57**, 2482 (1998).

[35] S. Heinrichs, J. Rottler, and P. Maass, Phys. Rev. B **62**, 8338 (2000).

[36] Z. Y. Zhang, X. Chen, and M. G. Lagally, Phys. Rev. Lett. **73**, 1829 (1994); Z. Y. Zhang and M. G. Lagally, Science **276**, 377 (1997).

[37] T. Zhang, J. Zhong, Z. Zhang, and M. G. Lagally, Phys. Rev. B **63**, 113403 (2001).

[38] O. Pierre-Louis, M. R. D'Orsogna, and T. L. Einstein, Phys. Rev. Lett. **82**, 3661 (1999).

[39] M. V. Ramana Murty and B. H. Cooper, Phys. Rev. Lett. **83**, 352 (1999).

[40] M. Esser, K. Morgenstern, G. Rosenfeld, and G. Cosma, Surf. Sci. **402-404**, 341 (1998).

[41] C. R. Stoldt, A. M. Cadhile, C. J. Jenks, J.-M. Wen, J. W. Evans, and P. A. Thiel, Phys. Rev. Lett. **81**, 2950 (1998); A. M. Cahhile, C. R. Stoldt, C. J. Jenks, P. A. Thiel, and J. W. Evans, Phys. Rev. B **61**, 4910 (2000).